Front. Earth Sci. 2023, 17(3): 797−817
https://doi.org/10.1007/s11707-022-1074-2

RESEARCH ARTICLE

Laboratory simulation of CO_2 immiscible gas flooding and characterization of seepage resistance

Jie CHI (✉)[1], Binshan JU[2,3], Wenbin CHEN[2,3], Mengfei ZHANG[1], Rui ZHANG[4], Anqi MIAO[4], Dayan WANG[4], Fengyun CUI[4]

1 School of Big Data and Fundamental Sciences, Shandong Institute of Petroleum and Chemical Technology, Dongying 257061, China
2 School of Energy Resources, China University of Geosciences (Beijing), Beijing 100083, China
3 Key Laboratory of Geological Evaluation and Development Engineering of Unconventional Natural Gas Energy, Beijing 100083, China
4 School of Chemical Engineering, Shandong Institute of Petroleum and Chemical Technology, Dongying 257061, China

Abstract CO_2 flooding can significantly improve the recovery rate, effectively recover crude oil, and has the advantages of energy saving and emission reduction. At present, most domestic researches on CO_2 flooding seepage experiments are field tests in actual reservoirs or simulations with reservoir numerical simulators. Although targeted, the promotion is poor. For the characterization of seepage resistance, there are few studies on the variation law of seepage resistance caused by the combined action in the reservoir. To solve this problem, based on the mechanism of CO_2, a physical simulation experiment device for CO_2 non-miscible flooding production manner is designed. The device adopts two displacement schemes, gas-displacing water and gas-displacing oil, it mainly studies the immiscible gas flooding mechanism and oil displacement characteristics based on factors such as formation dip angle, gas injection position, and gas injection rate. It can provide a more accurate development simulation for the actual field application. By studying the variation law of crude oil viscosity and start-up pressure gradient, the characterization method of seepage resistance gradient affected by these two factors in the seepage process is proposed. The field test is carried out for the natural core of the S oilfield, and the seepage resistance is described more accurately. The results show that the advancing front of the gas drive is an arc, and the advancing speed of the gas drive oil front is slower than that of gas drive water; the greater the dip angle, the higher the displacement efficiency; the higher the gas injection rate is, the higher the early recovery rate is, and the lower the later recovery rate is; oil displacement efficiency is lower than water displacement efficiency; taking the actual core of S oilfield as an example, the mathematical representation method of core start-up pressure gradient in low permeability reservoir is established.

Keywords laboratory simulation, viscosity, starting pressure gradient, CO_2 immiscible flooding, characterization of seepage resistance

Received March 15, 2023; accepted April 10, 2023

E-mail: chijie7980@163.com

1 Introduction

At present, the research on CO_2 flooding seepage experiments in low permeability reservoirs is still in its infancy, and there are few mature theories. Among them, the basic idea of indoor research was put forward on CO_2 flooding in the S oilfield (Li et al., 2000). CO_2 non-miscible flooding test was carried a out on Daqing ultra-low permeability reservoirs, providing theoretical guidance for reservoir exploitation that is difficult to effectively drive underwater injection development conditions (Jiang et al., 2008). Although the CO_2 flooding field test carried out in China has certain guiding significance for improving the recovery efficiency of low permeability reservoirs, it does not give good instructions for the optimization of process parameters. An extra-low permeability reservoir in the periphery of Daqing Oilfield and determined the optimal injection-production parameter combination scheme from the aspects of gas injection rate, gas injection cycle, and production pressure was studied (Wen et al., 2015).The reservoir numerical simulator CMG was used to run the injection-production mode optimization simulation of the low permeability reservoir, optimized the injection-production mode in CO_2 flooding, and verified it by the reservoir numerical model of low permeability reservoir in the H87-2 block of Jilin Oil Field (Li et al., 2010a). Most of the previous

researchers carried out field tests in actual reservoirs or used reservoir numerical simulators for simulation. Due to the different stratigraphic structures and original substances of reservoirs, the field tests or simulations for a certain reservoir are targeted, but the promotion is poor. Based on the mechanism of CO_2 non-miscible flooding and following the similarity principle, a physical simulation experiment system for the CO_2 non-miscible flooding production method is designed. Two displacement schemes of gas flooding water and gas flooding are adopted, in view of formation dip angle, gas injection position, gas injection velocity, and other factors, to study the mechanism and characteristics of non-miscible gas flooding. Simulating development well pattern deployment through small holes on the glass panel, the gas injection well and the production well are selected, Simulation of reservoir dip angle by flat model dip angle and the gas injection equipment is adjusted to inject gas at a certain speed. The gas seepage process, the change of the gas drive front position, the gas dominant seepage channel, the main direction of gas seepage, the sweep position, and the gas swept range is observed, and the displacement time is recorded. At the same time, the quality of the produced liquid at every moment is measured and the liquid recovery rate is calculated. The device can solve the technical problem that the existing technology cannot accurately simulate the inclined heterogeneous reservoir, and realize visual displacement. Providing an experimental method and device for determining non-miscible gas flooding production method. It provides a new experimental technology for oilfield development, which has certain innovations and makes up for the blank of laboratory physical simulation in the early stage of reservoir development. The promotion of CO_2 non-miscible flooding can also make full use of greenhouse gases, bury them underground, reducing CO_2 content in the atmosphere, in line with the national carbon peak and carbon neutral strategy, meet the requirements of green low carbon development.

For the previous characterization of low permeability reservoir seepage resistance, the main influencing factors are boundary layer, injection rate, reservoir permeability, crude oil viscosity change, starting pressure gradient, etc. Among them, the influence of boundary layer on seepage law is studied (Liu et al., 2011; Zhang et al., 2008). The change law of crude oil viscosity in CO_2 flooding is discussed (Wang and Guo, 1989; Guo et al., 1999; Li et al., 2010b). The experimental research and quantitative calculation of start-up pressure gradient, numerical simulation of low permeability reservoirs, and application of low permeability gas reservoirs were investigated (Feng et al., 2008; Xiong et al., 2009; Wang et al., 2013; Wang et al., 2014). A theoretical model of non-Darcy flow in CO_2 flooding low permeability reservoirs was established (Yang, 2011), and confirmed that the existence of starting pressure gradient is an important reason for difficult exploitation of low permeability reservoirs. The variation characteristics of seepage resistance gradient caused by starting pressure gradient in low permeability reservoirs are relatively mature, but there are few studies on the variation law of seepage resistance caused by crude oil viscosity and starting pressure. In this paper, based on the variation law of crude oil viscosity and the variation law of oil, gas (CO_2), and water start-up pressure gradient. A method for characterizing the seepage resistance gradient of CO_2 flooding under the combined action of crude oil viscosity and starting pressure in the seepage process is proposed. For the natural cores of the S oilfield, the correlation between the start-up pressure gradient of oil, water, and CO_2 and the permeability and fluid viscosity of specific low-permeability cores is studied through experimental means, and the mathematical representation method of the start-up pressure gradient of low-permeability reservoirs is established to describe the seepage resistance of formation fluid in seepage more accurately.

The indoor experimental simulation and seepage resistance characterization of CO_2 non-miscible gas flooding are carried out, for future promotion of low permeability reservoir CO_2 flooding design, and the experiment provides laboratory experimental reference and theoretical basis.

2 Main physical factors characterizing seepage resistance

2.1 Variation law of crude oil viscosity

In the process of CO_2 flooding, CO_2 dissolved in crude oil leads to a decrease in crude oil viscosity. The change of crude oil viscosity is important in fluid physical parameters, which greatly affects the formation seepage process. Therefore, to study the changing of crude oil viscosity during CO_2 flooding, scholars have done a lot of research work. An experiment was conducted on the viscosity of oil and gas mixture in CO_2 non-miscible flooding and gave a quantitative calculation method (Chung et al., 1988). The viscosity reduction of heavy crude oil by CO_2 injection was studied, and established an empirical correlation describing the change of viscosity with temperature and CO_2 injection pressure (Wang and Guo, 1989). The viscosity prediction method of oil and gas mixture under low permeability conditions were proposed (Li and Guo, 1990). The experimental measurement of high-pressure viscosity of CO_2 injection system in Jianghan Oilfield was carried out (Wang and Guo, 1994). The water injection development process reservoir physical characteristic change rule research was carried on (Deng et al., 1996). a viscosity model based on PR state equation was established (Guo et al., 1999; Guo et al., 2009). The change of crude oil viscosity in the

process of water and oil contact was studied (Sun et al., 2003). The viscosity-temperature characteristics of crude oil and crude oil containing CO_2 gas was experimentally studied, the viscosity of oil-gas mixture under different gas-oil ratios was measured, and the influence of CO_2 dissolved gas on the viscosity of crude oil was analyzed (Geng et al., 2004). A mathematical simulation method for the influence of crude oil viscosity change on water flooding development was proposed (Ju et al., 2006). The viscous fingering characterization method and influencing factors of CO_2 non-miscible flooding were nalyzed (Li et al., 2010a). The influencing factors of CO_2 on the change of crude oil viscosity through long core physical simulation experiment was studied (Yang, 2011; Ying, 2012). Many scholars have carried out fruitful research on the change model of crude oil viscosity, and have obtained many new understandings. The influence of CO_2 on crude oil viscosity is mainly reflected in formation pressure, formation temperature and formation crude oil density. The influence of formation pressure and temperature on crude oil viscosity is mainly. Another important aspect is reflected in the quantitative calculation of crude oil viscosity in CO_2 flooding process. The quantitative calculation method by experimental measurement (Chung et al., 1988).

2.2 Variation law of starting pressure gradient of fluid

Theoretical studies show that fluid seepage in porous media is often accompanied by some physical and chemical effects, which have a great impact on the seepage law. When oil and water flow in the reservoir, in addition to the viscous resistance, there is another additional resistance, namely the adsorption resistance of oil and rock or the attraction resistance of hydration film. Only when the driving pressure overcomes this additional resistance, the liquid can flow, which is the starting pressure phenomenon. The porosity and permeability parameters of low permeability reservoirs are very low, and it is difficult to effectively drive the fluid in the formation only by using natural energy. To study the flow characteristics and laws of fluid in low permeability reservoirs, researchers have done a lot of experiments. According to the experimental results, the theoretical model of non-Darcy flow in low permeability reservoirs is established, and it is proved that the existence of starting pressure gradient is an important reason for the difficult exploitation of low permeability reservoirs. Only when the displacement pressure gradient is greater than the starting pressure gradient of the fluid in the formation, the reservoir can be effectively used. The law of reservoir starting pressure and established the corresponding expression was studied (Sun et al., 1998). In the same year, the oil-water two-phase flow theory and development index calculation method with the starting pressure gradient was studied (Deng and Liu, 1998). Two-phase seepage analysis of reservoirs with threshold pressure gradient were carried out (Song and Liu, 1999), and also carried out one-dimensional instantaneous pressure analysis of low permeability medium with threshold pressure gradient in the same year. The experimental study of low permeability sandstone reservoir seepage starting pressure gradient was carried out (Lv et al., 2002). A new method to solve the threshold pressure gradient of ultra-low permeability reservoirs was proposed (Li et al., 2004). In the same year, the physical simulation and numerical simulation methods of ultra-low permeability reservoir considering starting pressure gradient was studied (Han et al., 2004). A three-dimensional three-phase seepage numerical simulation method with variable starting pressure gradient was conducted (Zhao, 2006). In the same year, numerical simulation of coalbed methane plume horizontal well mining considering the starting pressure gradient was carried out (Zhang et al., 2006; Zhang et al., 2011). A new method to solve the starting pressure gradient of low permeability reservoirs was realized (Xu et al., 2007). The unsteady seepage model of low permeability gas reservoir considering starting pressure gradient was established (Feng et al., 2008). The pseudo-start pressure gradient of low permeability reservoirs was studied (Xiong et al., 2009). The seepage characteristics of low-flow reservoirs considering the start-up pressure and pressure sensitivity effect were studied (Jiang et al., 2009). A new method to determine the starting pressure gradient of low permeability core gas was proposed (Li et al., 2013a). The unsteady pressure analysis of low permeability medium with starting pressure gradient was studied (Wang et al., 2014). This part includes experimental study and quantitative calculation of starting pressure gradient, numerical simulation of low permeability reservoir, and application of low permeability gas reservoir. In general, the starting pressure gradient cannot be ignored for low-permeability and ultra-low-permeability reservoirs.

2.3 Mechanism of CO_2 non-miscible flooding

CO_2 non-miscible flooding means that the formation conditions do not meet the conditions that CO_2 and crude oil are miscible, part of CO_2 is dissolved in crude oil, which reduces the viscosity of crude oil and the surface tension. At the same time, the volume of crude oil expands to achieve the purpose of displacing crude oil. When the reservoir is not suitable for CO_2 miscible flooding, CO_2 non-miscible flooding can improve oil recovery to some extent. The field application of CO_2 non-miscible flooding mainly includes: ① restoring the pressure of depleted reservoir by CO_2. In general, recovery of reservoir pressure by CO_2 injection is slower than by water injection, but free gas will be generated in the reservoir, so that CO_2 can contact more crude oil and

increase the sweep efficiency of gas flooding. ② Gravity stabilized CO_2 non-miscible flooding. ③ Exploiting heavy oil reservoirs. The main flooding mechanism of CO_2 non-miscible flooding is to reduce the viscosity of crude oil, expand the volume of crude oil, extract and vaporize light hydrocarbons in crude oil, and reduce surface tension.

1) Reducing crude oil viscosity

When CO_2 is dissolved in crude oil, the viscosity of crude oil decreases significantly depending on pressure, temperature, and initial viscosity. In general, the higher the initial viscosity of crude oil, the higher the percentage of viscosity reduction after CO_2 dissolution. After the crude oil is saturated with CO_2, if the pressure is further increased, the crude oil viscosity will increase due to the compression effect.

2) Improving the flow ratio

After a large amount of CO_2 is dissolved in crude oil and water, crude oil and water will be carbonated. The viscosity of crude oil decreases after carbonation. The relevant tests at 45°C and 12.7 MPa showed that the solubility of CO_2 in water was 5% (mass) and that in crude oil was 15% (mass). After CO_2 is dissolved in crude oil, the viscosity of crude oil decreases, the volume of crude oil increases, and the fluidity of crude oil increases. CO_2 is dissolved in water. After water carbonation, the viscosity of water increases, thereby reducing the flow rate of water. According to some relevant literatures, CO_2 dissolved in water can increase the viscosity of water by 20%. Because after carbonation, the fluidity of crude oil and water tends to be close, it can improve the fluidity ratio of oil and water, thereby expanding the swept volume. The general black oil model does not include the solubility of natural gas in the water phase, but for the CO_2 non-miscible flooding black oil model, the solubility of CO_2 in water cannot be ignored (Ying et al., 2012).

3) Volume expansion of crude oil

A certain volume of CO_2 dissolved in crude oil, depending on pressure, temperature, and oil composition can increase the volume of crude oil by 10%–100%. The expansion coefficient depends on the mole fraction of CO_2 and the relative molecular mass of crude oil. CO_2 dissolves in crude oil, which expands the volume of crude oil and increases the kinetic energy in the liquid, thus improving the oil displacement efficiency.

4) Extraction and vaporization of light hydrocarbons in crude oil

When the pressure exceeds a certain value, CO_2 can extract and vaporize light hydrocarbons in different components of crude oil. Mikael S B and Palmer F S analyzed the crude oil produced by CO_2 miscible flooding reservoir in Louisiana and found that CO_2 first extracted and vaporized light hydrocarbons in crude oil, then heavier hydrocarbons were vaporized and finally stabilized. Extraction and vaporization are important mechanisms of CO_2 miscible flooding.

In tertiary oil recovery, the mechanism of residual oil displacement by CO_2 after water flooding remains to be further studied. At present, there are two possible mechanisms.

I) The expansion of crude oil, the destruction of capillary force balance caused by the change of oil-water curved surface, and the redistribution of phase lead to the flow of crude oil.

II) If the water phase is completely displaced, crude oil contacts directly with CO_2, reducing viscosity and expanding crude oil, increasing the internal energy of crude oil, and leading to enhanced oil recovery. No matter what kind of action, it needs sufficient time to make CO_2 molecules fully diffuse into crude oil.

5) Reducing surface tension

The experimental results show that residual oil saturation decreases with the decrease of oil-water surface tension. Most oil-water surface tension is 10–20 mN/m. To make residual oil saturation tend to zero, the oil-water surface tension must be reduced to 0.001 mN/m or lower. When the oil-water surface tension is reduced to less than 0.04 mN/m, the recovery factor will be significantly improved. The main role of CO_2 flooding is to extract and vaporize the light components in crude oil. A large number of light hydrocarbons and CO_2 are mixed, which can greatly reduce the oil-water surface tension, reduce the residual oil saturation, and thus improve the oil recovery.

6) Dissolved gas drive

A large amount of CO_2 dissolves in crude oil and has the effect of gas flooding. The mechanism of depressurized oil recovery is similar to that of dissolved gas flooding. With the decrease in pressure, CO_2 escapes from the liquid and produces a gas-driving force in the liquid, which improves the oil displacement effect. In addition, some CO_2 displacing crude oil will occupy part of the pore space and form bound gas, which can also help increase crude oil production.

7) Increasing permeability

Carbonated crude oil and water not only improve the fluidity ratio of crude oil and water but also help to inhibit clay expansion. After CO_2 is dissolved in water, it is weakly acidic and reacts with the carbonate of the rock skeleton, improving the formation's permeability. It can be seen that carbonate reservoirs are more suitable for CO_2 flooding.

3 Laboratory simulation of CO_2 non-miscible flooding

3.1 Experimental principle

The physical simulation experiment was designed according to the similarity principle (Dai and Jin, 1999). Physical simulation refers to the simulation of the same

basic phenomenon. At this time, the model is the same as all the physical quantities of the prototype, and the physical essence is consistent. The difference is only that the size ratio of each physical quantity is different. Physical simulation is the simulation that keeps the physical essence consistent.

In this experiment, the artificial sand filling model was used to simulate the non-miscible gas flooding process, focusing on the embodiment of gas gravity differentiation and the influence of model parameters on the non-miscible gas flooding effect. Two displacement schemes of gas flooding water and gas flooding oil are adopted, the non-miscible gas flooding mechanism and oil displacement characteristics are mainly studied based on formation dip angle, gas injection position, gas injection rate, and other factors. Deployment of simulated development well pattern through small holes on the glass panel, the gas injection and the production well are selected. The dip angle of the flat model is set to simulate the dip angle of the reservoir. The gas injection equipment is adjusted to inject gas at a certain gas injection rate. The gas seepage process is observed, and the change of the position of the gas drive front, the gas dominant seepage channel, the main direction of gas seepage, the displacement position, and the range of gas sweep are observed. The displacement time is recorded. At the same time, the quality of the produced liquid at each time is measured, and the recovery rate of the liquid is calculated.

3.2 Model design

The experimental model is a flat plate model made of organic glass material. The specification of the flat plate model is 100 mm × 100 mm. The interior of the flat plate model is designed as a hollow structure, which can be filled with gravel to simulate the formation of a pore medium. 25 threaded holes are designed on the surface of the organic glass on one side of the model to simulate the injection-production well pattern of reservoir development. The flat plate model is designed to rotate 360° around the bearing, which can be used to simulate the formation dip angle. The model design is shown in Fig. 1 when the organic glass is immersed in the corresponding fluid, the internal gravel can be fully saturated with the fluid, and the location of the gas injection well and the production well can be freely selected. For example, the top thread hole can be used for top gas injection, and the bottom thread hole can represent the production well.

The plate model has good permeability, which is very conducive to observing the gas-liquid displacement process through the surface. The characteristics of the model are that the displacement process is visualized and the operation is simple. Since the design thickness of the model is small, it can better simulate the displacement process of non-miscible gas flooding in two-dimensional sandstone reservoirs. The gas injection displacement mechanism is mainly studied for reservoir parameters such as formation dip angle, gas injection velocity and gas injection position. Table 1 is the parameter table for the model.

Fig. 1 Experimental supplies.

3.3 Experimental preparation

3.3.1 Experimental supplies

Considering the high viscosity and poor fluidity of crude oil, and the experimental model can only be simulated under normal pressure, mineralized water was selected to replace crude oil in the early stage of the experiment. To simulate the salinity of formation water, an appropriate amount of NaCl was added into the distilled water to prepare a solution with a salinity of 2.5 g/L, and its viscosity was 1 mPa·s. At the later stage of the experiment, ordinary white oil was selected with a viscosity of 5 mPa·s. The injected gas used is air. The experiment selected 80–120 mesh gravel, as shown in Fig. 2 to make the gravel in the model fully saturated solution, the model filled with gravel is placed in the solution for one day.

3.3.2 Determination of permeability and porosity

1) Permeability measurement

Using Darcy's formula of vertical linear steady seepage, permeability is measured by downward seepage with pressure head h. The determination method is shown

Table 1 Model parameters

Parameter	Length/cm	Width/cm	Thickness/cm
Exterior	50	50	0.5

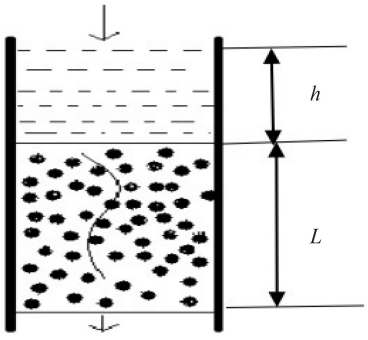

Fig. 2 the schematic diagram of the experimental apparatus for measuring permeability.

in Fig. 2.

According to darcy's formula:

$$Q = \frac{KA(p_1 - p_2)}{\mu L} = \frac{KA\rho g(h+L)}{\mu L}, \quad (1)$$

$$K = 10^7 \frac{Q\mu L}{A\rho g(h+L)}. \quad (2)$$

Experimental steps

① the inner diameter of the glass tube was measured by a Vernier caliper;

② the density of water is 1 g/cm^3 and the viscosity of water is 1mPa·s;

③ the gravity acceleration is 9.8 m/s^2;

④ the appropriate screen was selected for plugging in the glass tube, and then a certain height of gravel was filled in the glass tube;

⑤ measuring the height of filled gravel with a ruler;

⑥ control of certain head pressure.

Measure three groups of experimental data (Table 2), and finally, take the average value.

2) Porosity measurement

A certain amount of sand gravel was added to the vector tube, and the volume of sand gravel was V_1. Then, using the rubber head dropper to add an appropriate volume of water into the vector tube, and the volume of water was V_2. The vector tube was placed for a day, and then the volume V_3 of the remaining gravel in the vector tube was observed. The reduced volume was $V_1 + V_2 - V_3$, and the porosity of sand gravel was ϕ:

$$\phi = \frac{V_1 + V_2 - V_3}{V_1}. \quad (3)$$

Table 2 gravel permeability data

groups	1	2	3
q (cm^3)	0.20	0.21	0.20
t (s)	51	51	50
Q (cm^3/s)	0.0039	0.0041	0.004
K (μm^2)	0.301	0.317	0.307

Note: the average permeability of gravel measured is 0.308 μm.

Measure three groups of experimental data (Table 3), and finally, take the average value.

3.4 Design ideas and experimental scheme

The self-designed visual sand-filling plate experiment model was used to simulate the seepage process of two-dimensional non-miscible gas flooding. To make the comparative analysis better, and reflect the difference between water and oil as displacing phases in the formation, the experiment was designed into two categories: gas flooding water and gas flooding. For each category, three groups of experiments were designed to compare and analyze the displacement effects of different gas injection speeds, reservoir dip angles and gas injection positions. The design ideas are as follows.

1) Design ideas

① The three groups of experiments were continuous gas injections. The changes in the front position of gas flooding, the dominant gas seepage channel, the main direction of gas seepage, the sweep position and the gas sweep range were observed, and the displacement time was recorded. At the same time, the quality of the produced liquid at each moment was measured, the changes in the recovery rate and recovery rate of gas flooding were calculated, and the final recovery rate of each group was calculated.

② In experiment 1 and experiment 2, the same gas injection velocity and the same gas injection position were used. Select two different reservoir dip angles, and the influence of different reservoir dip angles on the displacement effect is compared.

③ Experiment 1 and Experiment 3 adopted the same reservoir dip angle and the same gas injection position. Select two groups of different reasonable gas injection speeds, the influence of different gas injection speed on the displacement effect was compared.

2) Experimental scheme

Specific experimental programs as shown in Table 4.

3.5 Experimental phenomena and results analysis

3.5.1 Gas drive water

1) Experimental data

The experimental data of three groups are shown in Table 5, Table 6 and Table 7.

Table 3 Experimental data of gravel porosity

Groups	1	2	3
ΔV (cm^3)	3.3	4.5	3.8
$V1$ (cm^3)	12	16	13
ϕ	0.275	0.281	0.292

Note: measured average porosity of gravel is 28.2%.

Table 4 Experimental Scheme

Experiment 1	The dip angle of the reservoir is 30°, gas injection alone to the reservoir from top 3 well, the bottom 23 wells are liquid production wells, and the gas injection rate is 5.0 cm^3/s.
Experiment 2	The dip angle of the reservoir is 45°, gas injection alone to the reservoir from top 3 well, the bottom 23 wells are liquid production wells, and the gas injection rate is 5.0 cm^3/s.
Experiment 3	The dip angle of the reservoir is 30°, gas injection alone to the reservoir from top 3 well, the bottom 23 wells are liquid production wells, and the gas injection rate is 7.7 cm^3/s.

Figure 3 shows the laboratory experiment device designed and manufactured by ourselves for the physical simulation of carbon dioxide flooding. Figure 4 shows the observation of the gas flooding front during the gas-driven water experiment.

The main direction of gas seepage is basically along the line between the gas injection well and the production well, and the direction is pointed to the production well. Due to the uniform sand filling, the front edge of the gas drive advancing in an arc. The advance speed is faster along the direction from the injection well to the production well, and the advance speed on both sides is slower.

2) Effect of different dip angles on displacement effects

Figure 5 shows the simulated dip angles of 30° and 45°, in the way of high injection and low recovery, and continuous gas injection, the relationship between recovery degree and injection volume ratio, through comparison can be seen: when the injection volume multiple is 94, the recovery degree under the condition of

Table 5 Gas flooding inclination angle of water 30° gas injection velocity 5.0 cm^3/s data

T (s)	0	20	60	96	120	152	193
E_R (%)	0	0.255	1.106	1.787	2.213	2.723	3.546
T (s)	222	252	279	322	351	380	410
E_R (%)	4.028	4.454	4.993	5.73	6.241	6.723	7.177
T (s)	440	471	502	534	567	600	633
E_R (%)	7.66	8.17	8.65	9.163	9.702	10.156	10.723
T (s)	667	701	736	773	811	849	888
E_R (%)	11.262	11.801	12.31	12.823	13.39	13.957	14.411
T (s)	927	968	1011	1052	1095	1141	1187
E_R (%)	14.95	15.489	16	16.567	16.851	17.418	18.411
T (s)	1284	1495	1672	1835	2094	2653	3376
E_R (%)	19.574	21.872	23.574	25.021	27.064	30.355	33.418
T (s)	3926	5132	5763	6588	7176		
E_R (%)	35.149	37.645	38.496	39.348	40.028		

Table 6 Gas flooding inclination angle of water 45° gas injection velocity 5.0 cm^3/s data

T (s)	0	17	51	89	122	169	204
E_R (%)	0	0.284	1.135	2.043	2.752	3.801	4.482
T (s)	248	282	329	365	416	469	524
E_R (%)	5.504	6.27	7.206	7.943	8.936	9.929	11.007
T (s)	581	642	706	774	846	943	1025
E_R (%)	12.113	13.135	14.213	15.262	16.312	17.447	19.035
T (s)	1112	1205	1306	1414	1532	1659	1800
E_R (%)	20.142	21.305	22.468	23.603	24.738	25.929	27.092
T (s)	1955	2129	2323	2544	2796	3091	3446
E_R (%)	28.17	29.504	30.95	32.426	33.844	35.348	36.823
T (s)	3874	4400	5110	6162	7045		
E_R (%)	38.326	39.773	41.191	42.667	43.83		

Table 7 Gas flooding inclination angle of water 30° gas injection velocity 7.7 cm^3/s data

T (s)	0	15	45	70	97	133	170
E_R (%)	0	0.255	1.305	2.014	2.723	3.773	4.709
T (s)	207	245	285	327	372	418	466
E_R (%)	5.73	6.723	7.66	8.652	9.702	10.723	11.801
T (s)	518	574	632	696	784	856	934
E_R (%)	12.596	13.504	14.27	15.092	16	17.078	18.27
T (s)	1018	1108	1206	1313	1430	1560	1704
E_R (%)	19.149	20.113	20.993	21.986	22.894	23.801	24.681
T (s)	1874	2044	2250	2485	2761	3090	3492
E_R (%)	25.589	26.468	27.348	28.227	29.106	30.043	30.95
T (s)	3978	4625	5562	6745			
E_R (%)	31.887	32.709	33.617	34.582			

Fig. 3 Physical simulation of carbon dioxide flooding.

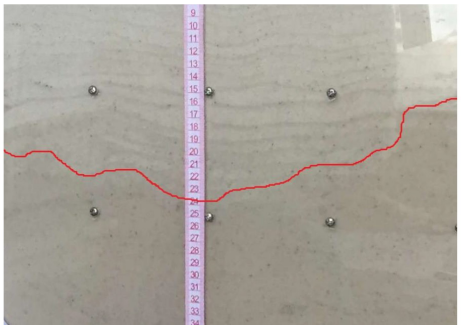

Fig. 4 Gas driving water of gas flooding front.

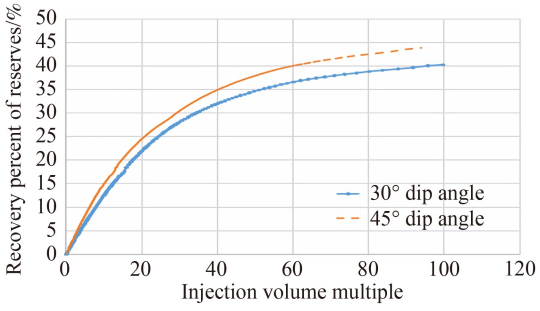

Fig. 5 Different strata dip angle and recovery degree.

continuous gas injection (high injection and low recovery) under the condition of simulated 45° formation dip is 3.8% higher than that under the condition of continuous gas injection (high injection and low recovery) under the condition of simulated 30° formation dip. This is mainly due to the fact that the density of air is much lower than that of water, and the larger the formation dip is, the more conducive the gas is to accumulate at the top, and the gravity separation of water and gas is obvious, so the recovery factor is large. This group of experiments showed that: reservoirs with a certain dip angle are favorable for gas flooding, and the greater the dip angle, the more favorable the gas forms the gas top at the top, and the displacement effect is better.

3) Influence of different gas injection speed on displacement effect

Figure 6 shows the simulated dip angle of 30° stratum, when the gas injection rates are 5.0 cm^3/s and 7.7 cm^3/s, respectively. The relationship between recovery and injection volume ratio, through comparison can be seen: at a higher gas injection rate, the early harvest rate is higher, but the final adoption is low. This is because at a higher gas injection rate, fast gas breakthroughs, forming gas channeling, not conducive to oil displacement, and the produced degree of the reserves is reduced. Therefore, the oilfields developed by gas injection, according to the

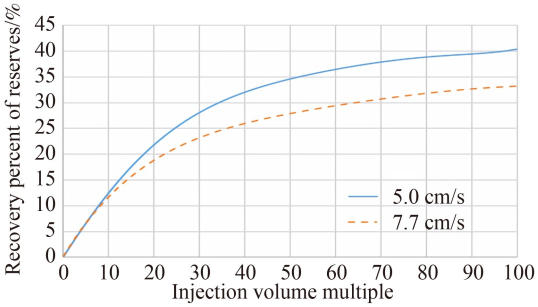

Fig. 6 Different gas injection velocity and recovery degree.

reservoir physical properties of the oilfield, combined with economic limit production constraints, determine the reasonable gas injection speed.

3.5.2 Gas drive oil

1) Experimental data

The experimental data of the three groups are shown in Table 8, Table 9 and Table 10.

Through the experimental data and observation of the phenomenon, the gas drive oil front also advances in an arc shape, and the connection direction between the gas injection well and the production propels rapidly. The main direction of gas seepage also basically follows the connection direction between the gas injection well and the production well, but the advance speed of the gas drive oil front is significantly slower than that of the gas drive water.

2) The effect of different gas injection speeds on the displacement effect

Table 8 Gas drive oil dip angle 30° gas injection velocity 5.0 cm^3/s data

Pv (f)	0	0.4	1.13	1.6	2.21	2.96	3.53
E_R (%)	0	0.19	0.63	0.89	1.19	1.63	1.91
Pv (f)	4.11	4.68	5.27	5.87	6.49	7.12	7.77
E_R (%)	2.23	2.54	2.85	3.13	3.44	3.77	4.08
Pv (f)	8.44	9.12	9.81	10.56	11.32	12.11	12.91
E_R (%)	4.43	4.77	5.11	5.45	5.82	6.13	6.49
Pv (f)	13.76	14.92	15.83	16.79	17.79	18.84	19.93
E_R (%)	6.84	7.21	7.77	8.15	8.52	8.9	9.31
Pv (f)	21.09	22.29	23.57	24.93	26.37	27.92	29.59
E_R (%)	9.69	10.08	10.49	10.87	11.27	11.67	12.04
Pv (f)	31.36	33.28	35.37	37.67	40.17	42.96	46.09
E_R (%)	12.43	12.82	13.21	13.61	14.01	14.4	14.81
Pv (f)	49.67	53.79	58.45	64.03	70.93	80.12	91.73
E_R (%)	15.22	15.62	16.03	16.45	16.83	17.26	17.67

Table 9 Gas drive oil dip angle 45° gas injection velocity 5.0 cm^3/s data

Pv (f)	0.32	0.93	1.28	1.77	2.4	2.85	3.31
E_R (%)	0.2	0.64	0.9	1.2	1.64	1.92	2.24
Pv (f)	3.76	4.23	4.71	5.21	5.72	6.25	6.8
E_R (%)	2.56	2.87	3.15	3.46	3.79	4.1	4.45
Pv (f)	7.36	7.93	8.56	9.2	9.87	10.55	11.28
E_R (%)	4.79	5.14	5.48	5.85	6.16	6.52	6.87
Pv (f)	12.32	13.11	13.95	14.83	15.76	16.73	17.77
E_R (%)	7.25	7.81	8.2	8.57	8.95	9.36	9.75
Pv (f)	18.85	20.01	21.25	22.57	24	25.55	27.2
E_R (%)	10.14	10.56	10.94	11.34	11.75	12.13	12.54
Pv (f)	29	30.97	33.15	35.53	38.2	41.21	44.67
E_R (%)	13.05	13.55	14.07	14.59	15.1	15.63	16.15
Pv (f)	48.67	53.21	58.67	65.45	74.52	86.01	
E_R (%)	16.68	17.21	17.75	18.26	18.81	19.34	

Table 10 Gas drive oil dip angle 30° gas injection velocity 7.7 cm^3/s data

Pv (f)	0.41	1.13	1.54	2.18	2.92	3.49	4.07
E_R (%)	0.19	0.63	0.89	1.19	1.63	1.91	2.23
Pv (f)	4.64	5.24	5.85	6.51	7.17	7.86	8.58
E_R (%)	2.54	2.85	3.14	3.45	3.77	4.08	4.43
Pv (f)	9.32	10.08	10.92	11.79	12.69	13.61	14.62
E_R (%)	4.77	5.07	5.34	5.64	5.88	6.16	6.44
Pv (f)	16.1	17.19	18.36	19.59	20.9	22.28	23.76
E_R (%)	6.76	7.24	7.56	7.84	8.15	8.48	8.79
Pv (f)	25.3	26.96	28.75	30.66	32.73	34.99	37.41
E_R (%)	9.1	9.44	9.74	10.07	10.4	10.69	11
Pv (f)	40.06	42.98	46.2	49.75	53.74	58.25	63.45
E_R (%)	11.32	11.63	11.96	12.28	12.6	12.93	13.26
Pv (f)	69.48	76.36	84.64	94.97	108.81	126.38	
E_R (%)	13.59	13.92	14.25	14.56	14.91	15.24	

Figure 5 shows two cases of gas flooding water and gas flooding oil, the dip angle is 30°, when the gas injection rates were 5.0 cm^3/s and 7.7 cm^3/s, respectively, relationship between recovery and injection volume ratio. It can be seen that for gas flooding oil, the higher the gas injection rate is, the lower the later recovery is. The reason is that the gas injection speed is too large to make the gas drive front break through too early, driving efficiency decreases. At different gas injection velocities, oil displacement efficiency is lower than water displacement efficiency. This is because the viscosity of white oil is greater than that of water, large seepage resistance, and the density of white oil is less than that of water, oil-gas density is smaller than oil-water density, the effect of gravity differentiation is also relatively weak.

3) Effect of different dip angles on displacement effects

Figure 6 gives two cases of gas flooding water and gas flooding oil, the gas injection rate is 5.0 cm^3/s, when the dip angles are 30° and 45°, respectively, relationship between recovery and injection volume ratio. It can be seen: For gas drive oil, the greater the dip angle is, the higher the oil displacement efficiency is. The reason is that the greater the dip angle, the more obvious the gravity differentiation. Under different stratigraphic dip angles, oil displacement efficiency is lower than water displacement efficiency. This is also because the viscosity of white oil is greater than that of water, large seepage resistance, white oil density is less than water density, the effect of gravity differentiation is weak.

Experimental process diagram and experimental effect diagram can been found in Figs 9 and 10.

3.6 Theoretical and practical significance of carbon dioxide immiscible gas flooding laboratory equipment

This experimental device can be used for laboratory physical simulation in the early stage of inclined reservoir development, It cannot only simulate multiple reservoir development parameters such as reservoir dip angle, gas

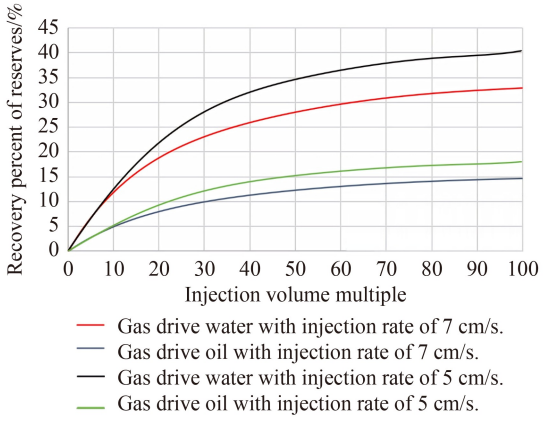

Fig. 7 Relationship between different gas injection velocities and recovery degree at 30° dip angle of formation.

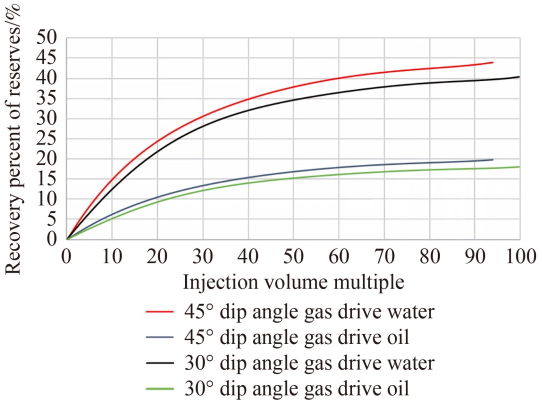

Fig. 8 Relationship between different dip angles of strata and recovery degree when gas injection rate is 5 cm^3/s.

injection position and gas injection velocity, but also simulate CO_2 non-miscible oil displacement mechanism, reservoir heterogeneity and reservoir injection-production well pattern. It can be widely used in physical simulation of non-miscible gas displacement characteristics and seepage law in inclined heterogeneous reservoirs in oilfield and oil-gas field development. It provides a new experimental technology for oilfield development, which is innovative to some extent, makes up for the blank of laboratory physical simulation in the early stage of reservoir development, and has a good application prospect.

A large number of domestic and foreign research and field applications have been proved, injection of CO_2 into oil layers can greatly improve oil recovery. This device is not only suitable for conventional reservoirs, but especially for low permeability and ultra-low permeability reservoirs. It can significantly improve oil recovery and has good social and economic benefits.

Promoting the use of CO_2 non-miscible flooding can also make full use of greenhouse gases, transfer and store them underground, reduce the content of CO_2 in the atmosphere, slow down the greenhouse effect, protect the atmospheric environment, meet the national carbon peak, carbon neutralization decision, and meet the requirements of green and low carbon development.

4 Characterization of inter well seepage resistance in CO_2 non-miscible flooding

In the process of CO_2 non-miscible flooding, due to the large amount of CO_2 dissolved in crude oil, the viscosity of crude oil changes continuously in the process of seepage, and the starting pressure gradient of crude oil also changes continuously. Therefore, the characterization of seepage resistance in the process of CO_2 non-miscible flooding must consider the changes of crude oil viscosity and starting pressure gradient.

4.1 Variation law of crude oil viscosity

For the influencing factors and prediction methods of oil-gas mixture viscosity in the process of CO_2 immiscible displacement, many scholars have conducted experimental studies. As mentioned above, the mechanism of CO_2 non-miscible flooding is mainly due to the decrease of crude oil viscosity and volume expansion caused by CO_2 dissolving (Chung et al., 1988). Studied the effects of different temperatures and pressures through experiments earlier, the relationship between the solubility of CO_2 in crude oil, swelling factor and viscosity of crude oil.

Under a certain fixed pressure, the viscosity of crude oil decreases with the increase in temperature, and its change with temperature is linear. The relationship between viscosity and temperature is

$$\lg\left(\frac{\mu_{T_2}}{\mu_{T_1}}\right)_{1\text{atm}} = 5707\left(\frac{1}{T_2}-\frac{1}{T_1}\right). \tag{4}$$

The viscosity of crude oil at other temperatures T_2 can be calculated by measuring the viscosity of crude oil at room temperature T_1, and the change of crude oil viscosity with temperature can be predicted by Eq. (4).

Under the condition of fixed temperature T, the function relation between crude oil viscosity and pressure is:

$$\lg\left(\frac{\mu_2}{\mu_1}\right)_T = A_T(P/14.7-1), \tag{5}$$

$$A_T = 13.844e^{4.633\gamma}/T^{2.17}. \tag{6}$$

The solubility R_s of CO_2 in formation crude oil is defined as standard volume of CO_2 per unit volume of ground-degassing crude oil can be dissolved in reservoir conditions.

Experiments show, the solubility R_s of CO_2 in crude oil increases with the increase of pressure, and decreases with temperature. It depends more on the change of pressure and temperature, the correlation with crude oil density is small. Therefore, solubility R_s is a function of formation pressure p, temperature T and crude oil density, which is most affected by p and T and less affected by γ.

$$R_s = \{0.178[a_1\gamma^{a_2}T^{a_7} + a_3T^{a_4}\exp(-a_5p - a_6/p)]\}^{-1}, \tag{7}$$

where each coefficient is $a_1 = 0.4936\times10^{-2}$, $a_2 = 4.0928$, $a_3 = 0.571\times10^{-6}$, $a^4 = 1.6428$, $a^5 = 0.6763\times10^{-3}$, $a^6 = -781.1334$, $a^7 = -0.2499$.

The expansion factor is defined as the ratio of crude oil volume of saturated dissolved CO_2 under reservoir temperature and pressure to crude oil volume of degassing under reservoir temperature and 1atm (0.101 MPa). For light oil, the volume expansion after CO_2 dissolution can reach twice the original volume, while for heavy oil, the expansion factor is much smaller. In general, the expansion factor of crude oil is a function of CO_2 solubility (Welker and Dunlop, 1963).

Generally speaking, the viscosity of crude oil is a function of crude oil components. For the mixture of CO_2 and crude oil, the function of viscosity concerning components is too complex, because the detailed components of crude oil cannot be accurately given, and the contribution of each component to the viscosity of oil-gas mixture cannot be accurately obtained, the mixture of CO_2 and crude oil is regarded as a two-phase two-component system. Therefore, the change in crude oil viscosity is related to the amount of CO_2 dissolved in crude oil. The higher the concentration of CO_2 dissolved in crude oil is, the smaller the viscosity of the oil-gas mixture is. The viscosity ratio of crude oil to CO_2 is very high, which can reach 10^3 orders of magnitude. If you know the viscosity of crude oil and CO_2, and the

concentration of CO_2 dissolved in crude oil can be obtained, so you can predict the viscosity of the mixture of CO_2 and crude oil (Sun, 1982; Lederer, 1993; Miller and Jones, 1981; Mehrotra and Svrcek, 1982).

The equation (Lederer, 1993) was verified accurately described the relationship between the viscosity of oil-gas mixture and the viscosity of two components and gas concentration in the system with high oil-gas viscosity ratio (Shu, 1982):

$$\ln\mu_{om} = X_o \ln\mu_o + X_s \ln\mu_g, \tag{8}$$

among them,

$$X_s = V_s/(\alpha V_o + V_s), \tag{9}$$

$$X_o = 1 - X_s, \tag{10}$$

$$\alpha = 0.225\gamma^{-4.16} T_r^{1.85}\left[\frac{e^{7.36} - e^{7.36}(1-p_r)}{e^{7.36}-1}\right], \tag{11}$$

among them, $T_r = T/547.57$, $p_r = p/1071$.

The volume fraction of CO_2 in oil-gas mixture can be calculated by the solubility and expansion factor of CO_2 in crude oil. The function relation of volume fraction X_S, CO_2 solubility R_s and expansion factor F_S is written as follows:

$$X_S = \frac{1}{\alpha F_{CO_2}/(F_o R_s)+1} = \frac{F_o F_s - 1}{\alpha + F_o F_s - 1}. \tag{12}$$

The viscosity of oil 4-1-1 to 4-1-9, the viscosity of the oil-gas mixture after CO_2 dissolved crude oil can be calculated. This result only needs to know the temperature, pressure and density of crude oil at a certain temperature and pressure.

Many scholars have developed various experimental methods, quantitative study on influencing factors of crude oil viscosity, and have successively obtained a variety of correlations.

Using RUSKA drop ball high-pressure viscosity meter, the viscosity change of heavy crude oil at different temperatures and different CO_2 injection pressure was measured (Wang and Guo, 1994), and established the empirical formula of crude oil viscosity change with temperature and pressure:

$$\ln\mu = 60.17585 - 0.287976T + 0.350313\times10^{-3}T^2 - 0.242256p + 0.158853\times10^{-3}p^2 + 0.616557\times10^{-3}T^2P^2. \tag{13}$$

The empirical Eq. (13) to the crude oil samples of the Jianghan Oilfield was applied (Wang and Guo, 1994), and measured their viscosity under reservoir conditions and the changes of viscosity with temperature and pressure after CO_2 injection under reservoir conditions.

Based on the method of (Chung et al., 1988; Li et al., 2010b) corrected the viscosity of crude oil after CO_2 dissolution, and applied it to the calculation of CO_2 non-miscible flooding numerical simulation.

4.2 Oil, gas (CO_2), water start-up pressure gradient change rule

Non-miscible gas flooding is widely used in medium-high permeability and low permeability reservoirs. The process of gas flooding in low permeability reservoirs is more complex, because the pore throat of low permeability reservoirs is small, and the seepage resistance of fluid is large, there is a starting pressure gradient, and it is accompanied by factors such as gas dissolution, phase transformation and miscible effect. Therefore, the seepage mechanism of gas flooding in low permeability reservoirs is more complex than that in medium-high-permeability reservoirs and water flooding. It can be said that medium-high permeability reservoirs are a simple case of low permeability reservoirs. In the process of gas flooding in low permeability reservoirs, the displacement pressure gradient must be greater than the starting pressure gradient. Only when the fluid in the formation can flow, an effective oil displacement system can be established.

4.2.1 Factors affecting start-up pressure gradient

In general, in medium and high permeability reservoirs, the starting pressure gradient is rarely considered, but when considering the seepage process of low permeability reservoirs, the starting pressure gradient of fluid must be considered. To study the factors affecting the start-up pressure gradient of low permeability reservoirs, scholars have done a lot of experiments and obtained typical non-Darcy flow curves. Through the nonlinear section on the curve, it is known that there is a start-up pressure gradient in the process of non-Darcy flow. Non-Darcy seepage characteristic curve is shown in Fig. 9.

As shown in Fig. 9. The typical non-Darcy flow curve is divided into a non-flow section (oa section), a nonlinear flow section (ae section) and a pseudo-linear flow section (ef section). Because the traditional method can only measure the def segment start pressure gradient value, starting pressure gradient $(\Delta p/L)_a$ can be obtained by extrapolation based on curve trend. When the displacement pressure gradient is less than $(\Delta p/L)_a$, the fluid cannot flow, showing a non-flow section oa; when the displacement pressure gradient is just greater than $(\Delta p/L)_a$, the fluid has just begun to flow, showing a nonlinear seepage section ae. A point displacement pressure gradient $(\Delta p/L)_a$ is defined as the minimum starting pressure gradient. When the displacement pressure gradient is greater than $(\Delta p/L)_c$, the fluid presents a quasi-Darcy seepage section ef. Point c displacement pressure gradient $(\Delta p/L)_c$ is defined as the

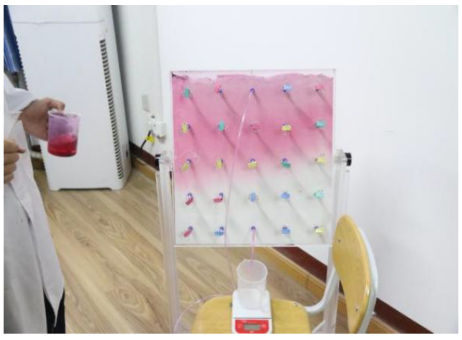

Fig. 9 Experimental process diagram.

maximum starting displacement gradient, i.e. critical displacement pressure gradient. Point e is the boundary point between the non-Darcy flow section and quasi-linear flow section, so the apparent starting pressure gradient $(\Delta p/\mathrm{L})_\mathrm{b}$ of point e is defined as the critical starting pressure gradient.

The rock pore medium structure, the surface properties of the rock pore wall, wet ability and fluid properties and other factors jointly determine the starting pressure gradient of the fluid, and the seepage mode does not affect the pore medium structure, the surface effect of the pore medium inner wall and the properties of the fluid. Therefore, the seepage mode does not change the size of the starting pressure gradient of the fluid. For a fixed fluid and pore medium, the starting pressure gradient is constant.

Through experiments, starting from the parameters of permeability, viscosity of crude oil, bound water and wettability, the influence factors of starting pressure gradient in low permeability reservoir are studied. The following conclusions are obtained: the threshold pressure gradient of low permeability reservoirs decreases with the increase of rock permeability, and increases with the increase of crude oil viscosity. For rock media with the same permeability, the stronger the lipophilicity is, the greater the starting pressure gradient during water flooding is. When the pore medium contains bound water, the measured value of the starting pressure gradient will be larger. Therefore, the use of rock samples containing bound water can better simulate the actual underground situation of low permeability reservoirs in the laboratory (Wang et al., 2006).

Therefore, the factors affecting the start-up pressure gradient of low permeability reservoirs include: the physical properties of the rock pore medium, fluid properties, and surface effect of the pore medium inner wall. The physical property of rock pore medium mainly refers to permeability, and the physical property of fluid mainly refers to the viscosity of fluid. Generally speaking, the surface effect of a specific reservoir medium is constant, so the starting pressure gradient research should focus on the permeability and viscosity.

4.2.2 Relationship between starting pressure gradient and seepage field, pore medium and fluid physical properties

1) Relationship between starting pressure gradient and seepage field

The key to developing low permeability reservoirs is to establish an effective oil displacement system, and make the fluid overcome the starting pressure gradient. The effective pressure gradient is an important standard to evaluate whether the reservoir is used or not. The effective pressure gradient is the difference between the displacement pressure gradient and the starting pressure gradient. Only when the displacement pressure gradient is greater than the starting pressure gradient, the fluid in the formation can flow. The effective pressure gradient expression is

$$\frac{\Delta p}{\Delta L}=\frac{\mathrm{d}p}{\mathrm{d}r}-\frac{\Delta p_\mathrm{o}}{\Delta L}. \tag{14}$$

For radial nonlinear seepage in low permeability reservoir, the pressure gradient distribution:

$$\frac{\mathrm{d}p}{\mathrm{d}r}=\frac{1}{r}\frac{(p_\mathrm{Rwf}-p_\mathrm{wf})\left[1-\dfrac{\sqrt{\dfrac{\phi}{2K}}\tau_\mathrm{o}(r_\mathrm{H}-r_\mathrm{w})}{p_\mathrm{Rwf}-p_\mathrm{wf}}\right]}{\ln\dfrac{r_\mathrm{H}}{r_\mathrm{w}}}+\sqrt{\frac{\phi}{2K}}\tau_\mathrm{o}. \tag{15}$$

The distribution of effective pressure gradient between injection and production wells is shown in Fig. 10. Through Eq. (10), it is found that the pressure gradient $\mathrm{d}p/\mathrm{d}r$ is inversely proportional to r, and the larger r is, the smaller $\mathrm{d}p/\mathrm{d}r$ is. The smaller the well spacing between the injection well and the production well, the higher the displacement pressure gradient is, and the greater the effective pressure gradient. Near the pit shaft, the displacement pressure gradient is high, the farther away from the pit shaft, the smaller the displacement pressure gradient. When the well spacing is too large, the effective pressure gradient is zero, and the effective displacement pressure system cannot be established, which is not conducive to reservoir utilization.

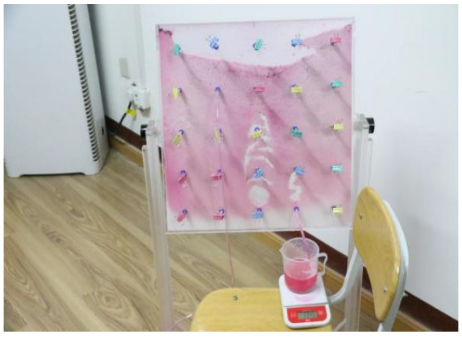

Fig. 10 Experimental effect diagram.

The utilization degree of movable oil is an important index to evaluate the effective utilization of reservoirs, within the limited oil supply radius, the relationship between the utilization degree of movable oil and the effective displacement pressure gradient is (Li et al., 2013b):

$$F = 1 - \frac{5.714}{\sqrt{K}} \times \frac{A}{\left(\frac{\Delta p}{\Delta L}\right)^n} + \frac{8.613}{K} \times \frac{A^2}{\left(\frac{\Delta p}{\Delta L}\right)^{2n}}. \quad (16)$$

The effective pressure gradient distribution of the square five point well pattern and the reservoir utilization are shown in Fig. 11. There is a high pressure gradient center of the injection well and four high pressure gradient centers of production wells in the square five-point well pattern, the points in the pressure field of injection and production wells are all low pressure gradient centers. When the pressure difference is small and the displacement pressure gradient is small, the effective pressure gradient is zero, as shown in Fig. 11(a), and the reservoir cannot be used; when the pressure difference increases to a certain extent, the effective pressure gradient is greater than zero, and the reservoir is from unconnected to usable, as shown in Fig. 11(b) ; as the pressure difference continues to increase, the effective pressure gradient continues to increase, and the reservoir is used more, as shown in Fig. 11(c) .

2) Relationship between starting pressure gradient and physical properties of porous media and fluid

The main factors affecting the starting pressure gradient of low permeability reservoirs are the physical properties of rock pore medium and fluid. The physical properties of rock medium mainly refer to permeability, and the physical properties of fluid mainly refer to the viscosity of fluid.

① Permeability of rock pore medium

The relationship between starting pressure gradient and permeability of porous media, the predecessors have done a lot of research (Sun et al., 1998; Deng and Liu, 1998; Song and Liu, 1999; Lv et al., 2002). The starting pressure gradient and permeability are in a linear relationship on the double logarithmic curve, the empirical formula of the relationship is obtained by regression (Huang, 1998):

$$G = \frac{\Delta P_o}{\Delta L} = aK^{-n}. \quad (17)$$

In the above formula, α and n are constants. If the physical properties of different reservoirs are different, the values are different. According to the empirical formula, as long as the corresponding regression coefficient is determined, the starting pressure gradient of the reservoir can be obtained.

It can be seen from Figs. 12 and 13, the smaller the permeability is, the greater the starting pressure gradient. When the permeability decreases to a certain value, the starting pressure gradient will increase sharply. It can be seen that for low permeability reservoirs, the formation permeability has a great influence on the starting pressure gradient.

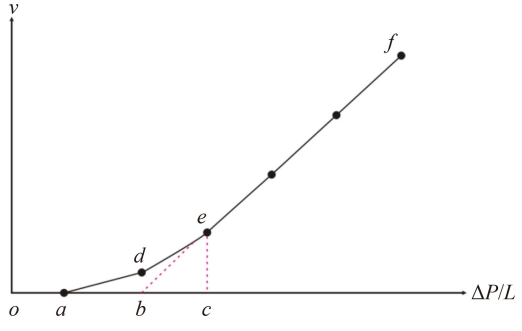

Fig. 11 Typical low velocity non-Darcy seepage characteristic curve (Si, 2006).

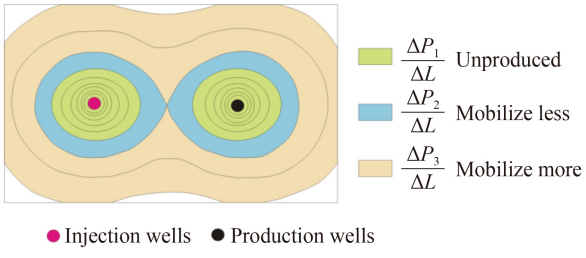

Fig. 12 Distribution of effective pressure gradient between injection and production wells.

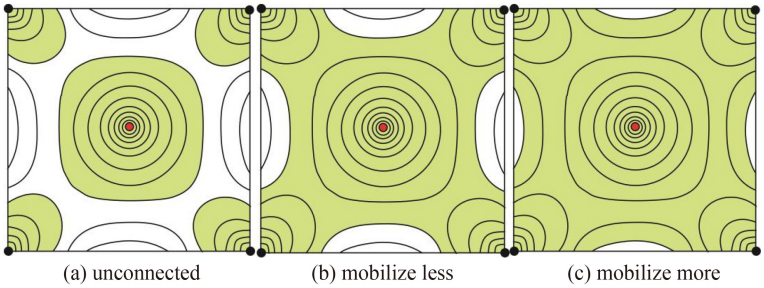

Fig. 13 distribution and utilization of effective pressure gradient between injection and production wells ($\Delta P_1 < \Delta P_2 < \Delta P_3$).

② Viscosity

Generally speaking, it is believed that both heavy oil reservoirs and low permeability reservoirs have high starting pressure gradient. The seepage of fluid in porous media belongs to non-Darcy seepage, but the mechanism of non-Darcy seepage caused by high starting pressure gradient is different (Sun, 2010). Low permeability reservoir lies in low permeability, the viscous oil reservoir is because the high viscosity of crude oil forms a strong viscous force between crude oil and the inner wall of pore medium, non-Darcy seepage is formed. The results show that, the relationship between starting pressure gradient and pore medium and fluid is

$$\frac{\mathrm{d}p_0}{\mathrm{d}L} = \sqrt{\frac{\phi}{2K}}\tau_0, \tag{18}$$

among them,

$$\tau_o = f(\mu \cdot C \cdot K \cdot T\frac{\Delta p}{\Delta L}), \tag{19}$$

where τ_0 is restricted by the interaction of solid-liquid interface, so the interaction of solid-liquid interface also affects the starting pressure gradient. The higher the viscosity of crude oil, the greater the viscous force, the greater the starting pressure gradient, as shown in Fig. 14.

③ Fluidity

In the non-Darcy flow process, the start-up pressure gradient is related to the permeability of porous media and the viscosity of fluid, and the fluidity is the ratio of permeability to viscosity. Considering these two factors together, the relationship between the start-up pressure gradient and the fluidity can be obtained (Yang et al., 2010). There is also a good linear relationship between the start-up pressure gradient and the fluidity on the double logarithmic diagram, as shown in Fig. 15. The relationship is

$$\ln\frac{\Delta P_o}{\Delta L} = a - b\ln\frac{K}{\mu}, \tag{20}$$

in the above formula, a and b are constants, and the values are different for different crude oil properties.

For low permeability reservoirs, the threshold pressure gradient is a factor that must be considered, and the threshold pressure gradient is closely related to the permeability of pore medium and the viscosity of fluid. Therefore, the influencing factors of starting pressure gradient and its mathematical representation are studied, it is of great significance for the characterization of seepage resistance in low permeability reservoirs.

4.2.3 Mathematical characterization of starting pressure gradient in low permeability reservoir

Through previous research work, startup pressure gradient logarithmic curve display, the starting pressure gradient keeps a linear relationship with permeability. In fact, many domestic low permeability reservoir core laboratory experiments, several empirical formulas of starting pressure gradient and permeability have been established as follows:

$$G = \frac{\Delta P_o}{\Delta L} = aK^{-n}, \tag{21}$$

among them,

S oilfield: $G = K^{-0.865}/3.596$,

Changqing oilfield: $G = 0.0608K^{-1.1522}$,

Chaoyang Valley oilfield: $G = 0.1164K^{-0.8567}$,

Yushulin oilfield: $G = 0.2K^{-0.5161}$.

4.2.4 Non-Darcy seepage natural core experiment

On the basis of previous research work, aiming at the actual core of S oilfield, the correlation between oil, water, CO_2 start-up pressure gradient and specific low permeability core permeability and fluid viscosity is studied by experimental means. Mathematical characterization method of core starting pressure gradient in low permeability reservoir is established, the seepage resistance of formation fluid seepage is described more precisely.

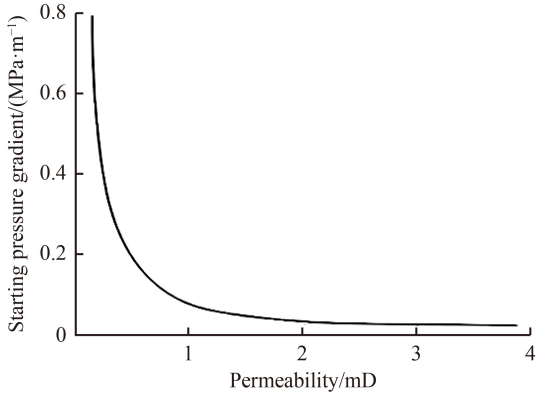

Fig. 14 Starting pressure gradient versus permeability curve (Huang, 1998).

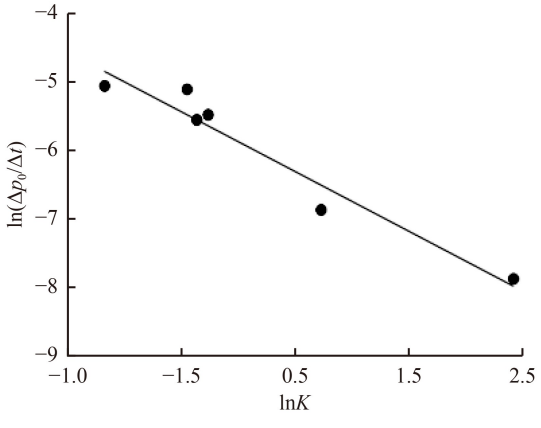

Fig. 15 tart pressure gradient and permeability double logarithmic relationship (Lv et al., 2002).

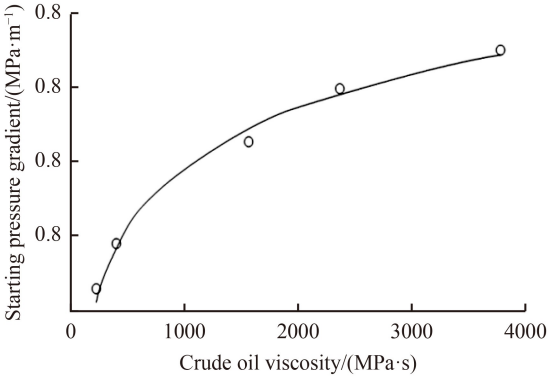

Fig. 16 Relationship between crude oil viscosity and starting pressure gradient (Sun et al., 2010).

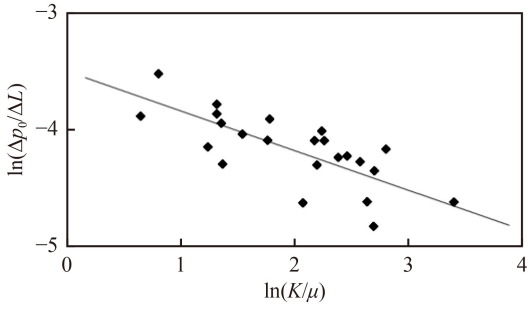

Fig. 17 Double logarithmic relationship between starting pressure gradient and flow rate (Yang et al., 2010).

1) Experimental equipment and methods

Experimental standard: SYT6703-2007, SYT5345-2006.

Experimental device: core displacement system, constant temperature device, high pressure sample storage container, core holder, etc.

Experimental core: S oilfield natural core.

Experimental conditions: preparation of formation water according to actual salinity, the total salinity of formation water is 29818 mg/L, the water type is $CaCl_2$.

Simulated oil is prepared from crude oil and aviation kerosene, the simulated oil viscosity is 1.5 mPa·s at 142°C.

Back pressure: 10 MPa, temperature: 142°C (simulated actual formation temperature), while ensuring that CO_2 viscosity is basically consistent with the actual reservoir conditions.

2) Experimental steps

According to the relevant industry standards SYT6703-2007 'core flow test instrument general technical conditions', SYT5345-2006 'oil-water relative permeability determination', the main steps are as follows.

① Testing of core porosity and permeability

The porosity and permeability of rock samples in this experiment were measured.

② Non-Darcy seepage test

Step 1: measure the geometric parameters of five cores and determine the basic parameters of porosity and permeability;

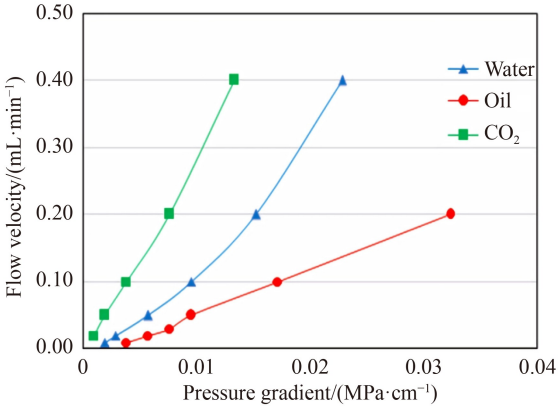

Fig. 18 Non-Darcy flow characteristic curve of core 1.

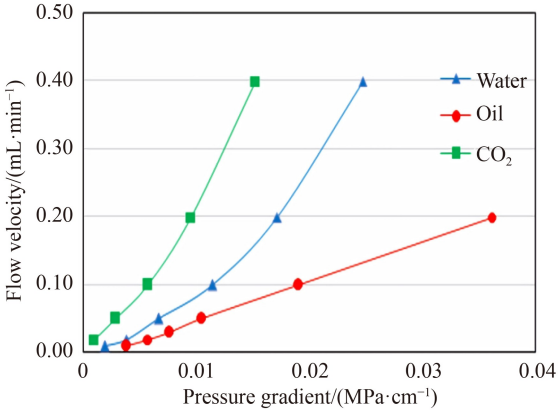

Fig. 19 Non-Darcy flow characteristic curve of core 2.

Step 2: saturate five cores with simulated formation water (salinity 29818 mg/L);

Step 3: measure the velocity of formation water passing through five rock samples with different permeability, and draw the relationship curve between velocity and injection-production pressure difference;

Step 4: in the experimental temperature (142°C), simulated oil with viscosity of 1.5 mPa·s, water flooding at 0.1 mL/min, until water does not produce;

Step 5: at the beginning of the experiment, the displacement was started at a flow rate of 0.01 ml/min, and the pressure at the inlet and outlet of the core holder was continuously recorded. After the inlet and outlet pressure is stabilized, the flow rate is gradually increased, until the complete non-Darcy seepage curve simulating oil displacement water is measured;

Step 6: after Step 5 is completed, CO_2 is used to drive oil at a flow rate of 0.1 mL/min, until the oil is no longer produced;

Step 7: start the displacement with 0.01 mL/min flow rate, record the pressure of the inlet and outlet of the core holder continuously, wait for the pressure of the inlet and

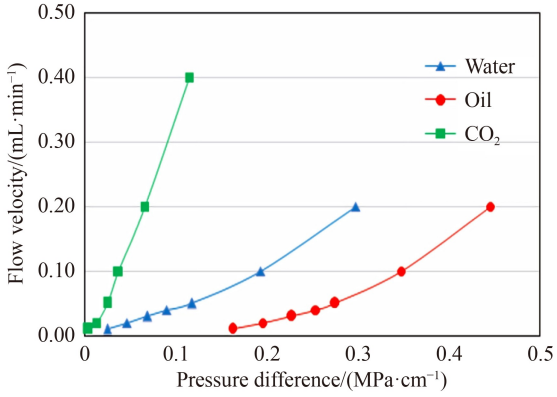

Fig. 20 Non-Darcy flow characteristic curve of core 3.

outlet to be stable, and then gradually increase the flow rate, until the complete non-Darcy percolation curve of gas drive oil is measured;

Step 8: replace rock samples, repeat steps 3 to 7, until the determination of all five rock samples is completed.

3) Test results

The non-Darcy seepage curves of five rock samples are as follows.

Due to the difference between the stress state and fracture factors of the ultra-low permeability core laboratory test and the actual situation of the formation, it is found that when the ultra-low permeability core 4 and core 5 are displaced, even if the minimum flow rate is 0.01 ml/min, it will still hold pressure at the inlet and outlet of the core holder, unable to reach the set flow. It is considered that the flow through these two rock samples is pseudo flow, the actual flow rate is much smaller, and the actual seepage curve should move downward, the experimental data of ultra-low permeability rock samples can be used as a reference.

According to the results of this experiment, refer to S oilfield core data in relevant literature, the relationship curve between the starting pressure gradient and permeability of the rock samples in this experiment is made, as shown in Figs. 21 and 22.

It can be seen from Fig. 22, the double logarithmic curve of starting pressure gradient and permeability shows a linear relationship, the functional relationship between starting pressure gradient and permeability is obtained by fitting:

Oil-phase threshold pressure gradient: $G = 0.83K^{-0.857}$,

Water starting pressure gradient: $G = 0.39K^{-0.842}$,

CO_2 start-up pressure gradient: $G = 0.102K^{-1.449}$.

It can be seen from Fig. 24, the bi-logarithmic curve of starting pressure gradient and fluidity also shows a linear relationship, the functional relationship between the start-up pressure gradient and the fluidity of the oil phase can be obtained by fitting:

$$G = 0.586\left(\frac{K}{\mu}\right)^{-0.857}. \tag{22}$$

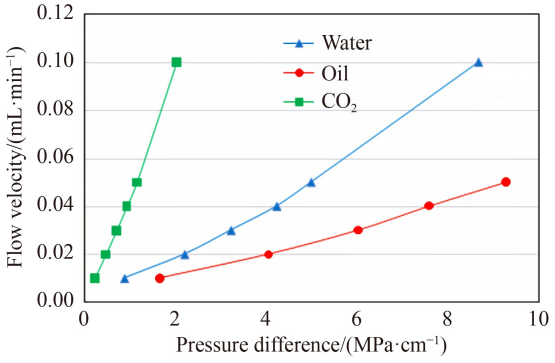

Fig. 21 Non-Darcy flow characteristic curve of core 4.

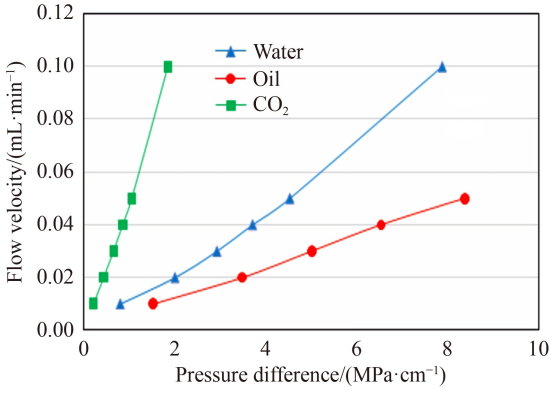

Fig. 22 Non-Darcy flow characteristic curve of core 5.

4.3 Establish effective displacement pressure system theory

When an effective displacement pressure system is established in the formation, the oil well begins to produce, and the formation pressure near the production well decreases rapidly. If the formation energy cannot be supplemented in time, the production will decrease, until an effective pressure system cannot be established in the formation, and the fluid in the formation cannot be driven. The effective displacement pressure system can keep the formation pressure stable, which is because the energy is added to the formation in time to maintain the balance of production and injection. According to the principle of seepage mechanics, the influencing factors of pressure system between injection and production wells include production, production pressure difference, well spacing, etc. The relationship between starting pressure gradient and injection-production well spacing has been studied, and the premise of determining injection-production well spacing is to establish an effective displacement pressure system. Under the condition of the limit well spacing, the displacement pressure gradient just overcomes the starting pressure gradient, and the fluid in the formation can flow exactly.

The establishment of an effective displacement pressure system is the guarantee of effective fluid utilization in

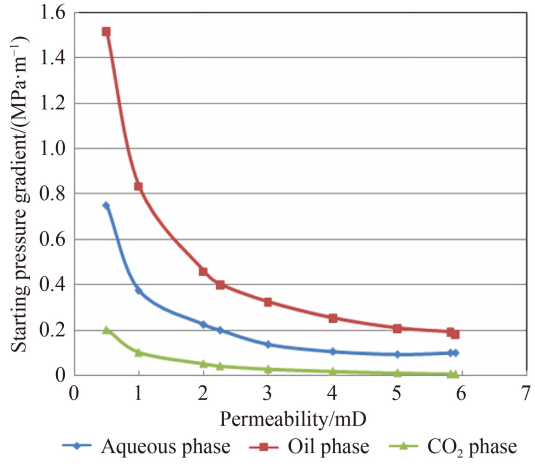

Fig. 23 Curves of relationship between starting pressure gradient and permeability.

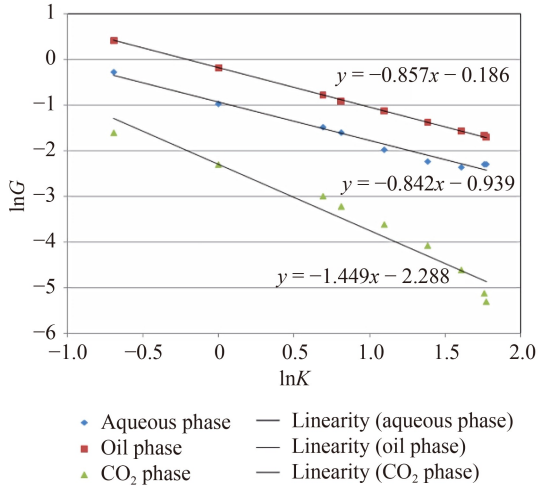

Fig. 24 Starting pressure gradient and permeability double logarithmic curve.

formation. The effective pressure gradient is the difference between the displacement pressure gradient and the starting pressure gradient, and it is the key to whether the fluid at any point in the formation can flow, it is also an important standard to evaluate whether the reservoir can be used. The relationship is as follows:

$$\frac{\Delta p}{\Delta L}=\frac{\mathrm{d}p}{\mathrm{d}r}-\frac{\Delta p_{\mathrm{o}}}{\Delta L}. \tag{23}$$

Using the superposition principle of potential, the pressure gradient distribution on the main flow line of the injection-production well is derived. The pressure gradient distribution formula on the main flow line of one source and one sink of output such as plane radial seepage is obtained as follows:

$$\frac{\mathrm{d}p}{\mathrm{d}r}=\frac{(p_{\mathrm{e}}-p_{\mathrm{w}})}{\ln(d/r_{\mathrm{w}})}\frac{d}{2r(d-r)}. \tag{24}$$

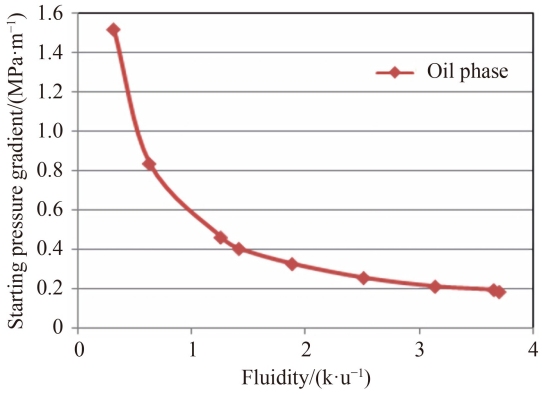

Fig. 25 Relationship curve between starting pressure gradient and fluidity.

From Fig. 25, it can be seen that the displacement pressure gradient near the injection-production well is very large. The farther away from the injection-production well, the displacement pressure gradient gradually becomes weak, and the displacement pressure gradient at the midpoint of the mainstream line is the smallest. Therefore, there must be a minimum displacement pressure gradient between injection wells and production wells, only when the minimum displacement pressure gradient is exactly equal to the starting pressure gradient in the oil layer, the effective displacement pressure system in the whole formation can just be established. The well spacing is the maximum well spacing that can establish the effective displacement pressure gradient, that is limit well spacing.

When the distance between injection and production wells is greater than the limit well spacing, the minimum displacement pressure gradient between injection and production wells is less than the starting pressure gradient, the formation cannot establish an effective displacement pressure system, and the fluid in the formation cannot flow. When the distance between injection and production wells is less than the limit well spacing, the displacement pressure gradient is everywhere greater than the starting pressure gradient, and an effective displacement pressure system can be established between injection and production wells.

5 Conclusions

1) From the observation of the displacement front, it can be seen that the main direction of gas seepage is basically along the line between the gas injection well and the production well, and the direction is pointed to the production well. The front edge of the gas drive is advancing in an arc. The advance speed is faster along the direction from the injection well to the production well, and the advance speed on both sides is slower, and the

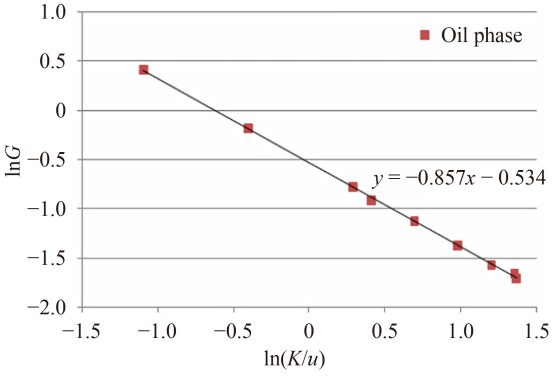

Fig. 26 Double logarithmic curve of starting pressure gradient and fluidity.

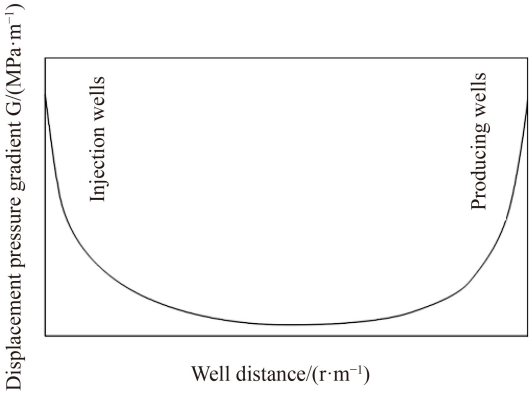

Fig. 27 Distribution of displacement pressure gradient (absolute value *G*) on main flow line between injection and production wells in low permeability reservoir.

advancing speed of the gas drive oil front is significantly slower than that of gas drive water.

2) For gas flooding water, under the condition of the same steam injection rate and different formation dip angles, when the injection volume multiple is 94, the recovery degree under the simulated 45° formation dip angle is 3.8% higher than that under the simulated 30° formation dip angle. So the reservoir with a certain formation dip angle is beneficial to the implementation of gas flooding, and the greater the formation dip angle, the better the displacement effect. Under the condition of the same dip angle and different gas injection speed, the greater the gas injection speed, the higher the early recovery rate, but the final recovery degree is low.

3) For gas drive oil, under the conditions of the same steam injection rate and different formation dip angles, the larger the formation dip angle, the higher the oil displacement efficiency; under the condition of the same dip angle and different gas injection rate, the higher the gas injection rate, the higher the early recovery rate and the lower the later recovery rate; the oil displacement efficiency is lower than the water displacement efficiency under different formation dip angles or different gas injection speeds.

4) For the oilfields developed by gas injection, according to the reservoir physical properties of the oilfield, combined with economic limit production constraints, determine the reasonable formation dip angle, gas injection speed, and gas injection position.

5) The experimental device can be used for laboratory physical simulation in the early stage of reservoir development. It cannot only simulate a variety of reservoir development parameters at the same time, but also simulate CO_2 miscible flooding mechanism and reservoir heterogeneity. It can be widely used in the physical simulation of non-miscible gas flooding characteristics and seepage law of inclined heterogeneous reservoirs in oilfield oil and gas field development, and can provide more accurate development simulation for practical field application. The promotion of CO_2 non-miscible flooding can also make full use of greenhouse gases, bury it underground, reducing CO_2 content in the atmosphere, in line with the national carbon peak, carbon neutral strategy, meet the requirements of green low carbon development.

6) The change of seepage resistance during CO_2 non-miscible flooding is characterized by the change of crude oil viscosity and starting pressure gradient. For the change of crude oil viscosity, under a certain fixed pressure, the crude oil viscosity decreases with the increase of temperature; under the condition of fixed temperature T, the viscosity of crude oil decreases with the increase of pressure, under the condition of formation dip angle and steam injection speed, the greater the viscosity of crude oil, the greater the seepage resistance gradient. The change in starting pressure is mainly related to permeability and fluid viscosity, that is, it is related to fluidity. The permeability makes the starting pressure gradient nonlinear. The smaller the permeability, the greater the starting pressure gradient. When the permeability drops to a certain value, the starting pressure gradient will rise sharply; the higher the viscosity of crude oil, the greater the viscous force, and the greater the starting pressure gradient. Only the displacement pressure gradient must be greater than starting pressure gradient, and the fluid in the formation can flow. Considering the permeability of porous media and fluid viscosity, it is obtained that the starting pressure gradient has a linear relationship with the double logarithm of fluidity.

7) To further verify the linear relationship between the start-up pressure gradient and the double logarithmic curve of the fluidity, for S oilfield actual core, conduct field tests, through experimental means, the relationship curve between the starting pressure gradient and permeability of rock samples in this experiment is obtained. The functional relationship between the start-up pressure gradient of oil, water and CO_2 and the permeability of the specific low permeability core is fitted as follows: $G = 0.83K^{-0.857}$, $G = 0.39K^{-0.842}$, $G = 0.102K^{-1.449}$; the functional relationship between oil

phase start-up pressure gradient and fluidity is as follows: $G = 0.586\left(\frac{K}{\mu}\right)^{-0.857}$.

8) The effective displacement pressure system can keep the formation pressure stable, the pressure system between injection and production wells is related to production, production pressure difference and well spacing. When the distance between injection and production wells is less than the limit well spacing, the displacement pressure gradient is everywhere greater than the starting pressure gradient. An effective displacement pressure system can be established between injection and production wells, and the fluid in the formation can be effectively driven.

Acknowledgments Parts of this work were supported by the Dongying Science Development Fund Project (Nos. DJ2022009 and DJ2020003), the Shandong Provincial Higher Education Research and Development Program (Science and Technology A Class) (No. J18KA201), the High-level Talent Research Start-up Fund of Shengli College of China University of Petroleum (No. KQ2019-008), the Chunhui Project of Shengli College of China University of Petroleum (No. KY2017004) and the Research Cultivation Project of College of Big Data and Basic Science of Shandong Institute of Petroleum and Chemical Technology (No. XYPY2201) which supports are appreciated. We also thank all editors and anonymous reviewers for their comments and suggestions.

Competing interests The authors declare that they have no competing interests.

Nomenclature

K—fluid measuring permeability, μm^2;

Q—liquid flow, cm^3/s;

L—height of gravel filled, cm;

A—section area, cm^2;

ρ—fluid density, kg/cm^3;

g—acceleration of gravity, m/s^2;

μ—liquid viscosity, mPa·s;

h—discharge head, m;

ϕ—porosity, %;

μ_{T_1}—*V*iscosity of crude oil at pressure 1 atm, temperature T_1, mPa·s;

μ_{T_2}—*V*iscosity of crude oil at pressure 1 atm, temperature T_2, mPa·s;

μ_1—*V*iscosity of crude oil at pressure of 1 atm (0.101MPa), mPa·s;

μ_2—*V*iscosity of crude oil at pressure p, mPa·s;

A_T—*P*roportion coefficient of temperature and crude oil density;

γ—crude oil density, kg/cm^3;

R_s—solubility, g;

T—temperature, °C;

P—pressure, pa;

V—volume fraction;

α—*E*mpirical coefficients of temperature, pressure and crude oil density;

F_S—inflation factor;

F_{CO_2}—the ratio of CO_2 volume under standard condition to the volume under reservoir temperature and pressure;

F_o—the ratio of the volume of crude oil under reservoir temperature and 0.1MPa pressure to the volume under reservoir temperature and reservoir pressure;

τ_o—*Y*ield stress of formation crude oil, N/m^2;

r_H—*O*il supply radius of well area, m;

R_w—*E*ffective oil supply radius, m;

F—the utilization degree of movable oil;

A—drainage area, m^2;

$\frac{\Delta p}{\Delta L}$—*E*ffective displacement pressure gradient, MPa/m;

n—*F*itting index;

τ_o—Shearing stress, MPa;

C—Fluid component content, %.

References

Chung F T H, Jones R A, Hai T N (1988). Measurements and correlations of the physical properties of CO_2/heavy-crude-oil mixtures. SPE15080, 3(3): 822–828

Deng Y Z, Wu S Y, Zhang G Z, Zong X W (1996). Change of reservoir physical properties during development by waterflood. Oil Gas Recove Techn, (04): 51–59+6

Deng Y E, Liu C Q (1998). Theory of oil-water flow through porous media and calculation of development indexes with starting gradient included. Petrol Explor and Develop, (06): 53–56+6+13

Dai Y S, Jin Z L (1999). Application of analogousness theory in simulate experiment. In: The 8th National Conference on Plastic Processing theory and New Technology, 26–27

Feng G Q, Liu Q G, Shi G Z, Lin Z H (2008). An unsteady seepage flow model considering kickoff pressure gradient for low-permeability gas reservoirs. Petrol Explor Develop, (04): 457–461

Guo X Q, Rong S X, Yang J T, Guo T M (1999). The viscosity model based on PR education of state. Acta Petrol Sin, (03): 64–69+6

Geng H Z, Chen J W, Sun R Y, Li D X (2004). Effect of dissolved carbon dioxide on the viscosity of crude oil. J U Petrol (Nat Sci Ed)(04): 78–80

Guo Y W, Yang S L, Li L C, Wang G, Zhao W X (2009). Experiment on physical modeling of displacement oil with natural gas for long core. Fault-Block Oil Gas Field, 16(6): 76–78

Huang Y Z (1998). Seepage Mechanism of Low Permeability Reservoir. Beijing: Petroleum Industry Publishing House, 80–86

Han H B, Cheng L S, Zhang M L, Cao Q Y, Peng D G (2004). Physical simulation and numerical simulation of ultra-low permeability reservoir in considering of starting pressure gradient. J U Petrol (Nat Sci Ed), (06): 49–53

Ju B S, Fan T L, Zhang J C, Wang X D (2006). Oil viscosity variation and its effects on production performance in water drive reservoir. Pet Explor Dev, (01): 99–102

Jiang H F, Lei Y G, Xiong X, Yan L P, Pi W F, Li X J, Yu C H (2008). An CO_2 immiscible displacement experimental aiming at Fuyang

extra-low permeability layer at peripheral of Daqing placanticline. Geoscience, (04): 659–663

Jiang L P, Li M, Jiang P, Lao Y C, Liu S Q (2009). A research on the seepage of low-permeability reservoirs under consideration of threshold pressure and pressure-sensitive effect: a case study of member L_1 member in Weixi' nan depression. China Offshore Oil Gas, 21(06): 388–392

Li B T, Guo T M (1990). Measurement and correlation of high pressure viscosities of reservoir crude oil. Pet Explor Dev, (06): 72–79

Lederer E L (1993). Mischungs-und verdünnungs viscosität. In: Proc., World Pet. Cong., London, 2, 526–28

Li Z Q, Li X Y, Yuan M Q, Huang D G, Zhang G G (2000). Study on laboratory experiments of CO_2 drive in Shang 13–22 unit. Oil Gas Recove Techn, (03): 9–11+5

Lv C Y, Wang J, Sun Z G (2002). An experimental study on starting pressure gradient of fluids flow in low permeability sandstone porous media. Pet Explor Dev, (02): 86–89

Li Z X, Han H B, Cheng L S, Zhang M L, Shi C E (2004). A new solution and application of starting pressure gradient in ultra-low permeability reservoir. Pet Explor Dev, (03): 107–109

Li Z F, He S L (2005). Influence of boundary layer upon filtration law in low permeability oil reservoirs. Petrol Geo Oilfield Develop Daping, (02): 57–59+77–107

Li B Z, Li X F, Kamy S, Yao Y D (2010a). Optimization of the injection and production Schemes during CO_2 flooding for tight reservoirs. J Southwest Petrol U (Sci and Techn Ed), 32(02): 101–107+203

Li D X, Su Y L, Gao H T, Geng Y H (2010b). Fluid parameter modification and affecting factors during immiscible drive with CO_2. J China U Petrol (Nat Sci Ed), 34(05): 104–108

Liu W D, Liu J, Sun L H, Li Y, Lan X Y (2011). Influence of fluid boundary layer on fluid flow in low permeability oilfield. Sci Techn Rev, 29(22): 42–44

Li Z C, Li M, Jiang Y J (2013a). A New method for determining gas threshold pressure gradient in low-permeability rock. J Southwest Petrol U (Nat Sci Ed), 35(03): 105–110

Li B, Tang H, Lv D L (2013b). Study on pressure gradient and producing degree of water flooding reserves in square inverted nine-spot well pattern. Lithologic Reservoirs Efficiency, 25(2): 95–99

Miller J, Jones R (1981). A laboratory study to determine Physical Characteristics of Heavy Oil after CO_2 Saturation. ln: SPE/DOE Enhanced Oil Recovery Symposium. Society of Petroleum Engineers

Mehrotra A K, Svrcek W Y (1982). Correlations for properties of bitumen saturated with CO_2, CH_4 and N_2, and experiments with combustion gas mixtures. J Can Pet Technol, 21(6): 95–104

Shu (1982). Viscosity correlation for mixtures of heavy oil, bitumen, and petroleum fractions. Soc Petrol Eng J, SPE-11280, (1): 277–282

Sun L J, Wu F, Zhao W H, Zhao L J (1998). The Study and application of reservoir start-up pressure. Exploration & Development Science Institute, ZPEB, (05): 30–33

Song F Q, Liu C Q (1999). Two-phase flow analysis of reservoir with starting pressure gradient. J U Petrol, (03): 60–63+69

Sun M R, Zhang X, Geng H Z (2003). Experimental study on viscosity variation of crude oil in oil-water contact pro-cess. J China U Petrol, (02): 63–66+5–4

Si D H (2006). How state distribution of areal radial flow in low permeability sandstone reservoir. Pet Explor Dev, (04): 491–494

Sun J F (2010). Threshold pressure gradient study on non-Newtonian flow of heavy oil reservoirs in Shengli Oilfield. Petrol Geol Recove Efficiency, 17(06): 74–77+116

Welker L R, Dunlop D D (1963). Physical properties of carbonated oils. JPT, 873–75. Trans, AIME: 228

Wang L S, Guo T M (1989). Study on heavy oil viscosity reduction by injection carbon dioxide. Pet Explor Dev, (06): 72–77

Wang L S, Guo T M (1994). High pressure viscosity measurement of Jianhan oil reservoir oil and its carbon dioxide injected system. J China U Petrol (Nat Sci Ed), (04): 125–130

Wang Y F, Wu G, An S K, Zhao W, Jin H (2006). Experimental study on influencing factors of start-up pressure gradient of permeability rocks. J Petrol Nat Gas, (03): 112–113+446

Wang Y N, Wu X D, Zhang S B, Lai F P, Teng M (2013). Experiment and effect evaluation of CO_2 immiscible displacement in Extra-low permeability reservoirs. J Oil Gas Techn, 35(04): 136–140+169

Wang X D, Luo W J, Hou X C, Wang J L (2014). Transient pressure analysis of multiple-fractured horizontal well in boxed reservoirs. Petrol Explor Develop, 41(01): 74–78+94

Wen X, Liu Y T, Tian S B, Liu Y F, Liu B (2015). Injection-production parameters optimization of CO_2 flooding in extra-low permeability reservoir. J Shaanxi U Sci Techn (Nat Sci Ed), 33(03): 116–120+134

Xu J H, Cheng L S, Zou Y, Ma L L (2007). A new method for calculating kick off pressure gradient in low permeability reservoirs. Petrol Explor Develop, (05): 594–597+602

Xiong W, Lei Q, Liu X G, Gao S S, Hu Z M, Xue H (2009). Pseudo threshold pressure gradient to flow for low permeability reservoirs. Pet Explor Dev, 36(02): 232–236

Yang Y D, Wei D M, Li M L (2010). Study on reasonable well spacing optimization of low permeability and low grade reservoir. J Oil Gas Techn, 32(03): 353–356

Yang J (2011). Research and application on non-Darcy flow theorial model for CO_2 flooding. The Dissertation for Doctoral Degree. Daqing: Northeast Petroleum University

Ying L A (2012). The mathematical modeling of black oil. Mathe Model App, 1(04): 1–4

Zhao G Z (2006). Numerical simulation of 3D and three-phase flow with variable start-up pressure gradient. Acta Petrolei Sinica(S1): 119–123+128

Zhang D L, Wang X H, Song Y (2006). Numerical simulation of pinnate horizontal well for coal-bed gas development in consideration of start-up pressure gradient. Acta Petrol Sin, (04): 89–92

Zhang P, Zhang L Z, Li W Y, Wang Y F (2008). Experimental on the influence of boundary layer on the low non-Darcy seepage law. J Hebei U Eng(Nat Sci Ed), (03): 70–72

Zhang X S, Xie X Q, Chen M F (2011). Study on reasonable spacing in low permeability and fault block reservoir. Petrol Geo Recovery Efficiency, 18(6): 94–96